2009

Tailoring Local Conductivity by the Formation of Ag Nanoclusters in SiO2 Xerogel Films

Ricky Caperton
Virginia Commonwealth University

Tailoring Local Conductivity by the Formation of Ag Nanoparticles in SiO_2 Xerogel Films

A thesis submitted in partial fulfillment of the requirements for the degree of Master of Science in Physics / Applied Physics at Virginia Commonwealth University.

By

Ricky J. Caperton, Jr.

B.S. in Physics

James Madison University, 2007

M.S. in Physics/Applied Physics

Virginia Commonwealth University, 2009

Directors:

Director: Massimo F. Bertino, Associate Professor, Department of Physics

Virginia Commonwealth University,

Richmond, Virginia, 23284

August 2009

Acknowledgments

For starters, I would like to thank Dr. Bertino who welcomed me to his group upon his arrival to VCU. He gave me a wide range of interesting topics to pursue while keeping me focused and driven. I would also like to thank Dr. Baski who has taught me nearly everything there is to know about the AFM. I also give thanks to Chuck Wingfield and Stephen Mutisya who were part of Dr. Bertino's group. They made working in the lab easy-going and fun; it was a pleasure working with them. Also, I would like to include members of the physics group: Michael Foussekis, Monika Ruchala, Crystal Baird, Joe Ferguson, Vincent Ong, Kristen Casalenuovo, Joy McNamara, and Anita Olsen. All of you are great people who made this an amazing experience for me during my time at VCU. Your friendship inside and outside of the department has helped give me motivation to make this all possible.

Table of Contents

List of Figures

Abstract

Tailoring Local Conductivity by the Formation of Ag Nanoparticles in SiO_2 Xerogel Films

By Ricky J. Caperton, Jr.

A thesis submitted in partial fulfillment of the requirements of the degree of Master of Science at. Virginia Commonwealth University, 2009.

Major Director: Massimo F. Bertino, Associate Professor, Department of Physics

Porous silicon dioxide thin films were produced via dip-coating and doped with Ag^+ by adding $AgNO_3$ to the dipping solution. Nanoparticles were formed within the pores of these films by UV exposure. Nanoparticle formation was confirmed by UV-visible spectroscopy and Transmission Electron Microscopy (TEM). Conductive Atomic Force Microscopy (CAFM) showed that the conductivity of the films decreased upon exposure to UV. This decrease in the conductivity is most likely due to the clustering of charge carriers. Initially, Ag^+ ions are attached to negatively charged pore walls in a dense packing network. Upon UV exposure (125 mW @ 266 nm), the Ag^+ ions are reduced to Ag metal and agglomerate to form clusters. The agglomeration creates gaps in the film that decrease its conductivity. This ability to tune film conductivity was used to create insulating patterns within conducting films. A calibration mask was placed over the films during UV exposure, and exposed regions with a minimum width of ~2 μm were detected as depressions with insulating behavior. The fabrication of photonic and plasmonic devices is being explored using this method.

Chapter 1: Sol-Gel Materials

1.1 Introduction

Sol-gel materials are currently being considered as building blocks for a wide variety of devices such as photonic crystals, thermal insulators, radiation collectors, low dielectric constant materials, and microfluidics components.[1] The optical properties of these materials can be controlled by adding chromophores or nanoparticles to control the index of refraction, absorption, and luminescence.[234] Amorphous silica used in sol-gels also attracts interest for the design of optoelectronic devices such as on-chip optical waveguide structures[5], antireflection coatings for optical applications[6], and membranes of controlled permeability for gas separation.[7] Sol-gel materials can be roughly divided into two categories which depend on the process used to remove the gelation solvent. When supercritical drying is employed, highly porous materials are obtained called aerogels. When the solvent evaporates in air, more compact and less porous materials known as xerogels result. Because of its simpler processing, xerogels are more common than aerogels, especially when thin films are considered. This work focuses exclusively on xerogel thin films.

1.2 Sol-gel Processes and Thin Film Production

The sol-gel process is the basis for thin film preparation. The key steps of the sol-gel process are hydrolysis of alkoxides followed by condensation, as shown in Fig. 1.1 for the reaction of tetramethylorthosilicate (TMOS) with water in a basic environment. After NH_4OH and H_2O are added, the hydroxide ion attacks the functional group of the TMOS. This results in silicon that is terminated with hydroxyl groups. The hydroxide ions then react to form H_2O and a network of SiO_2. In our experiments, we used an amino-terminated silane moiety, aminopropyltriethoxysilane (APTES), which yields NH_2 – terminated materials that can

efficiently coordinate Ag and Ag^+. Polymers having functional groups such as $–NH_2$ and –COOH have a high affinity for metal atoms.[8]

Materials: Mospec silicon (111) wafer, distilled water, $AgNO_3$ from EM Science, methanol, 99% tetramethylorthosilicate (TMOS) from ACROS, and 99% aminopropyltriethoxylsilane (APTES) from ACROS (see Fig. 1.2).

The substrate for the thin films is a silicon (111) wafer cut into pieces (1x1 cm^2) using a carbide scribe and cleaned with methanol. The method of preparation of nanoparticles in aqueous medium involves the reduction of a metal precursor salt using UV photons.[9] The $AgNO_3$ solution with typical concentrations of 1 mol L^{-1} (M) was prepared by dissolving $AgNO_3$ in distilled water. The water in the $AgNO_3$ solution hydrolyzes the TMOS to form a SiO_2 network. Because of APTES, the SiO_2 network is terminated with amino groups which coordinate Ag. Thin films were prepared by manually dipping the silicon substrates in the sol-gel solution. The dipping solution was prepared by adding chemicals in this order to a 5 mL vial: 3 mL methanol, 100 µL TMOS, 200 µL APTES, and 300 µL of $AgNO_3$ solution. The solution gelled quite rapidly (less than a minute). Unlike conventional bulk gel formation, the drying stage overlaps the gelation and aging stages, establishing only a brief time span for condensation reactions to occur.[10] Before gelation, two to three films were able to be produced. After the thin films are produced, they must sit in the dark for at least one day to allow any excess methanol and water vapor to evaporate. The structure of the final deposited film depends on the competition between evaporation (which compacts the film) and condensation reactions (which strengthens the film).[11] This step is very important, because unpredictable results will occur otherwise, as shown later.

Initially, the films were produced with tetraethylorthosilicate (TEOS). The resulting samples were cracked and very disordered. After adding APTES the films were still full of defects and therefore the TEOS was replaced with TMOS. Interestingly, thin films were unable to be produced with just TEOS/TMOS. With the stabilization of the films due to APTES, different ratios of APTES/TMOS were used. The ideal ratio was 2:1 (APTES:TMOS), but ratios of 2:1 to 1:3 can produce films.

1.3 Ultraviolet (UV) Exposure

After the films age, they are ready to be exposed to UV light to induce Ag nanocluster formation. To minimize vibrations from the environment, the exposure setup is mounted on a Newport ST-200 Series Smart Table with auto-tune damping. The UV exposure system is shown in Fig. 1.4 and consists of a 532-nm laser (continuous-wave Coherent Verdi, 1 W) which is frequency doubled to 266 nm by a Coherent laser (MBD266, 125 mW). The beam travels ~ 48 cm to a mirror where it is reflected 90°, travels 13 cm to a short-focal lens (5 mm), and then travels ~13 cm to a prism where it is bent downward to strike the sample. This setup expands the beam diameter from about 3 mm to 1 cm. For unpatterned films (used for IV measurements), the beam evenly distributed over the surface and the same sample was exposed for 1, 2, 3, 4, and 8 min. For patterned films, a mask/target was used over the sample and exposure times were 7 to 9 min.

1.4 Atomic Force Microscopy

The atomic force microscope (AFM) was invented in 1986 by Binnig, Gerber, and Quate and is used to measure the topography of a sample surface at the nanometer scale. The AFM can image a broad range of materials by measuring the force between a probe and surface. The probe in the AFM is a micro-machined cantilever with a tip at its end. In our experiments, two types of

metallized cantilevers from MikroMash were used: 1) stiffer cantilevers (NSC15 Ti-Pt) with a resonant frequency of 325 kHz and spring constant of 40 Nm^{-1}; and 2) softer cantilevers (NSC 14 Ti-Pt) with a resonant frequency of 160 kHz and spring constant of 5 Nm^{-1}. Data was acquired from two different AFM instruments from Veeco: an older Dimension 3100 AFM and a newer ICON AFM. In both instruments, the tip is initially brought into contact with the sample via a stepper motor. While in contact with the surface, the very small tip-sample force (~10^{-9} N) is then measured by monitoring the cantilever deflection using a "beam-bounce" method with a laser beam.[12] The AFM operates on the basic principle of Hooke's Law: $F = -kx$, where x is the cantilever deflection and k is the cantilever spring constant. Forces that can be measured with the AFM include mechanical, van der Waals, chemical, electrostatic, magnetic, and many more.

The two main modes of AFM operation are contact and tapping mode. In contact mode the tip is kept in continuous contact with the surface and the tip-sample force (or cantilever deflection) is kept constant using a feedback loop. Disadvantages of contact mode include lower resolution and possible sample damage, but contact mode is necessary for simultaneous measurement of sample conductance. Tapping mode is another mode of AFM operation where the cantilever oscillates at its resonance frequency and the tip "taps" the surface. In this case, the tip is not in continuous contact with the surface and the amplitude of the cantilever oscillation is kept constant. The resonance frequency is determined automatically using the AFM software. Tapping mode does not allow for conductive imaging but its resolution is superior and sample damage is minimized.

The AFM instrument has three main components: AFM 'head', sample chuck on x-y translation stage, and computer controlled electronics. The head consists of a piezoelectric scanner, cantilever/tip with its holder, laser, and photo detector. The cantilever is mounted in its

holder using a spring lever. The chuck is the base of the AFM which holds the sample with a magnetic mount. Computer software is used to move the chuck using an x-y translation stage. The control electronics scans the cantilever over the sample surface for imaging and maintains a constant tip-sample force by adjusting the cantilever z-height. This z-height is then plotted to generate a topographic image of the sample surface.

The detailed procedure for operating the AFM is documented and available for each instrument. A few procedural notes are included here, particularly differences between the DIII and Icon instruments. The knurled knob to lock the head in place is turned *counterclockwise* on the DIII but is turned *clockwise* on the Icon. On both instruments, the laser is aligned on the cantilever using the two knobs on top of the head, and aligned on the photodetector using the two knobs on the left of the head. The laser location in the software should be at (0,0) for tapping mode and (0,-2) for contact mode on the DIII, but at (0,0) for contact mode on the Icon. To optimize imaging, the user should adjust the deflection or amplitude setpoint (corresponds to tip-sample force), integral/proportional gain, and scan speed.

1.5 Conductive Atomic Force Microscopy (CAFM)

Conductive AFM is a variant of contact-mode AFM that uses a conductive cantilever to obtain simultaneous images of the surface topography and current. During data acquisition the tip is grounded and an external bias is applied to the sample. To detect the tip-sample current there are two types of current amplifiers: 1) CAFM module for more conductive samples which has a current range of ±1000 pA and sensitivity of 5 pA; and 2) TUNA module for less conductive samples with a range of ±100 pA and sensitivity of 1 pA. Common parameter settings for both the DIII and Icon are shown in Figs. 1.6 and 1.7 and include: force deflection setpoint (0.26 V,

0.50 V), integral gain (1.3, 15), and proportion gain (2.6, 30). The Icon has a lower maximum bias voltage (10 V) as compared to the DIII (12 V).

1.6 Current-Voltage Data

The advanced mode feature of CAFM can provide current-voltage (IV) curves for specific locations on the sample. Most IV curves in this work were obtained using the DIII since it has a higher DC bias. There are two methods for IV curves: point-shoot at one location (used here) and the matrix method for multiple locations.

Initially, the sample topography is obtained using an 8:1 aspect ratio to save time. Using the advanced mode feature (View -> Force Mode -> Advance), IV curves are then obtained at the center of the image using the following parameters: (see Fig. 1.8)

Ramp Channel: DC Sample Bias
Ramp Begin: -12V
Ramp End: +12V
Scan Rate: 0.2 Hz
Number of Samples: 256 (number of data points in measurement)
Average Count: 10 (number of averaged measurements)
Data Type: Tuna Current
Data Scale: 200 pA

The IV curves can be captured (or saved) using two different methods. When the measurement is in progress the capture button can be clicked and the status will indicate “Next”. When the measurement is complete the curve will be saved and the status will update to “Done”. The other method is to let the measurement finish and then click capture.

Chapter 1 Figures

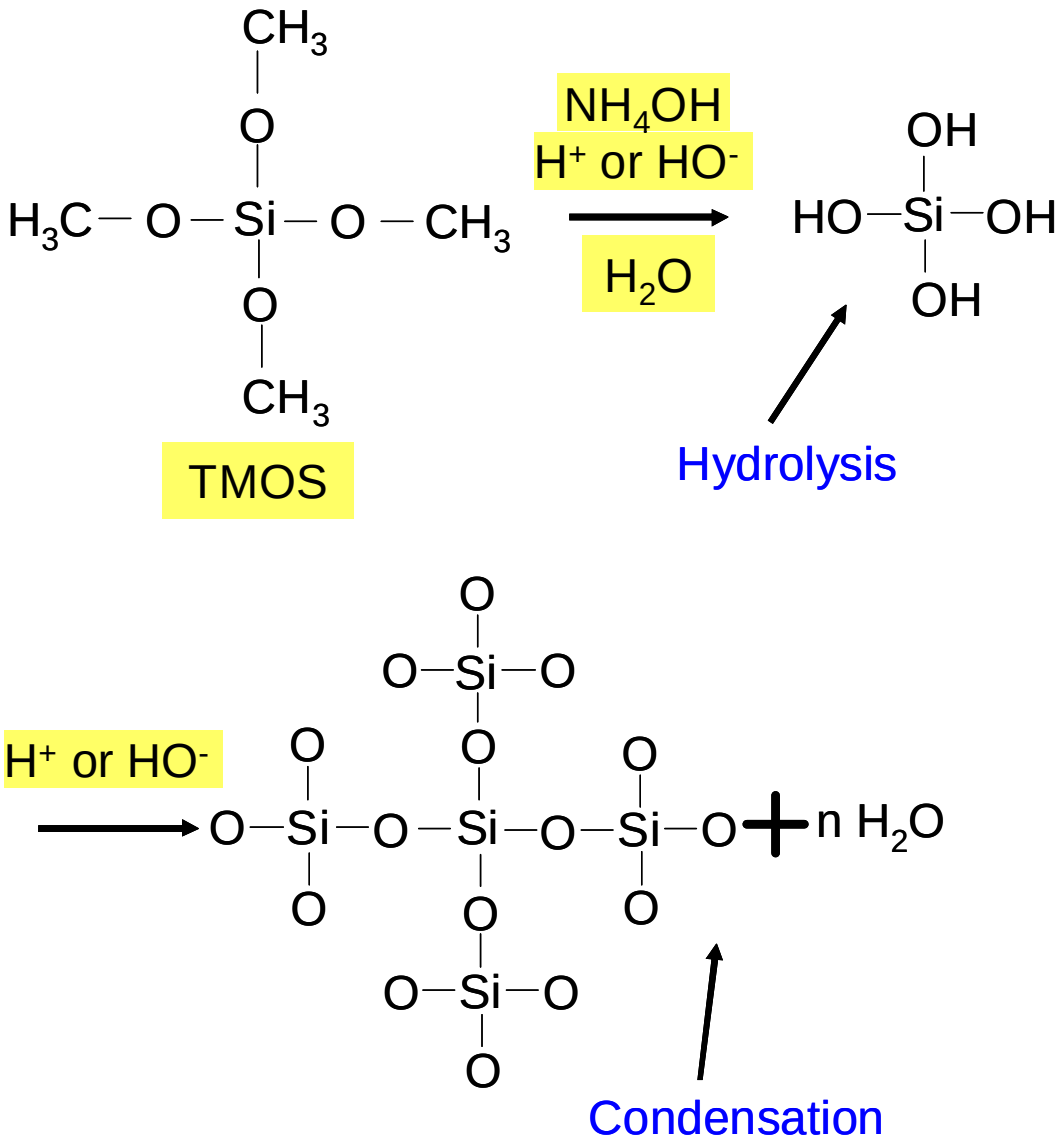

Fig. 1.1: Hydrolysis/Condensation reaction of tetramethylorthosilicate (TMOS).

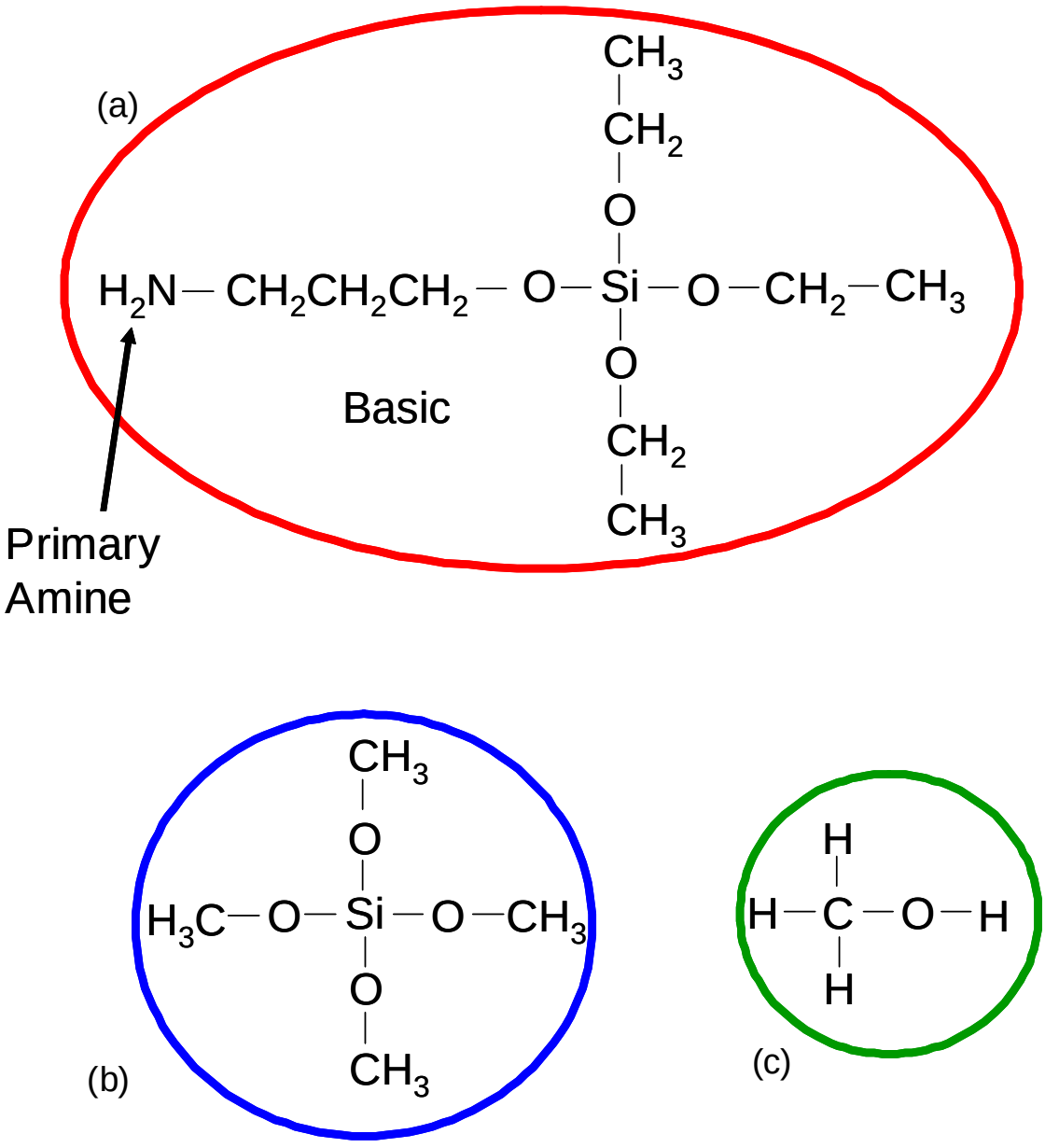

Fig. 1.2: (a) 3-aminopropyltriethylsilane, (b) tetramethylorthosilicate, and (c) methanol

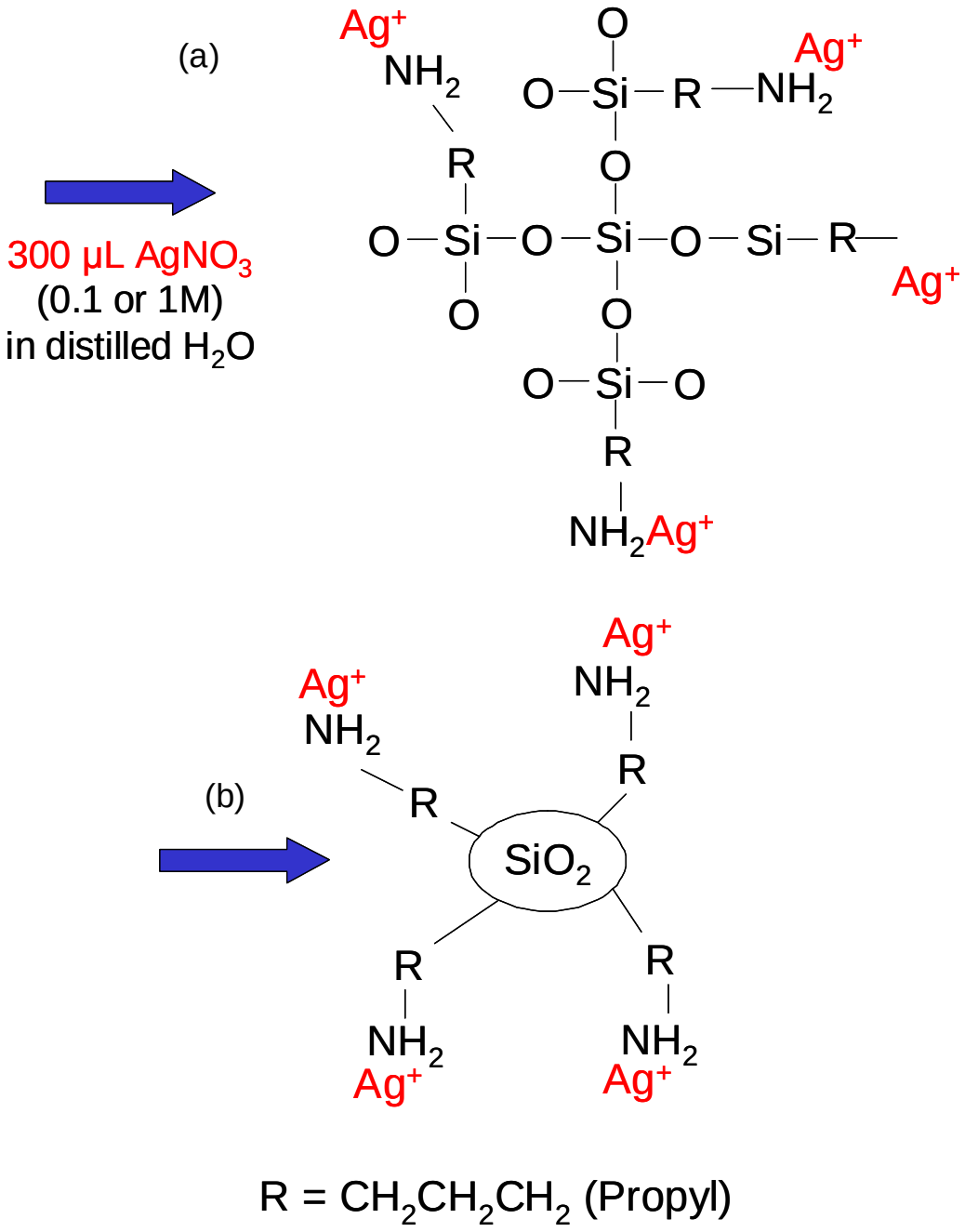

Fig. 1.3: (a) Hydrolysis of sol-gel to form network and (b) SiO_2 core terminated with NH_2 amine.

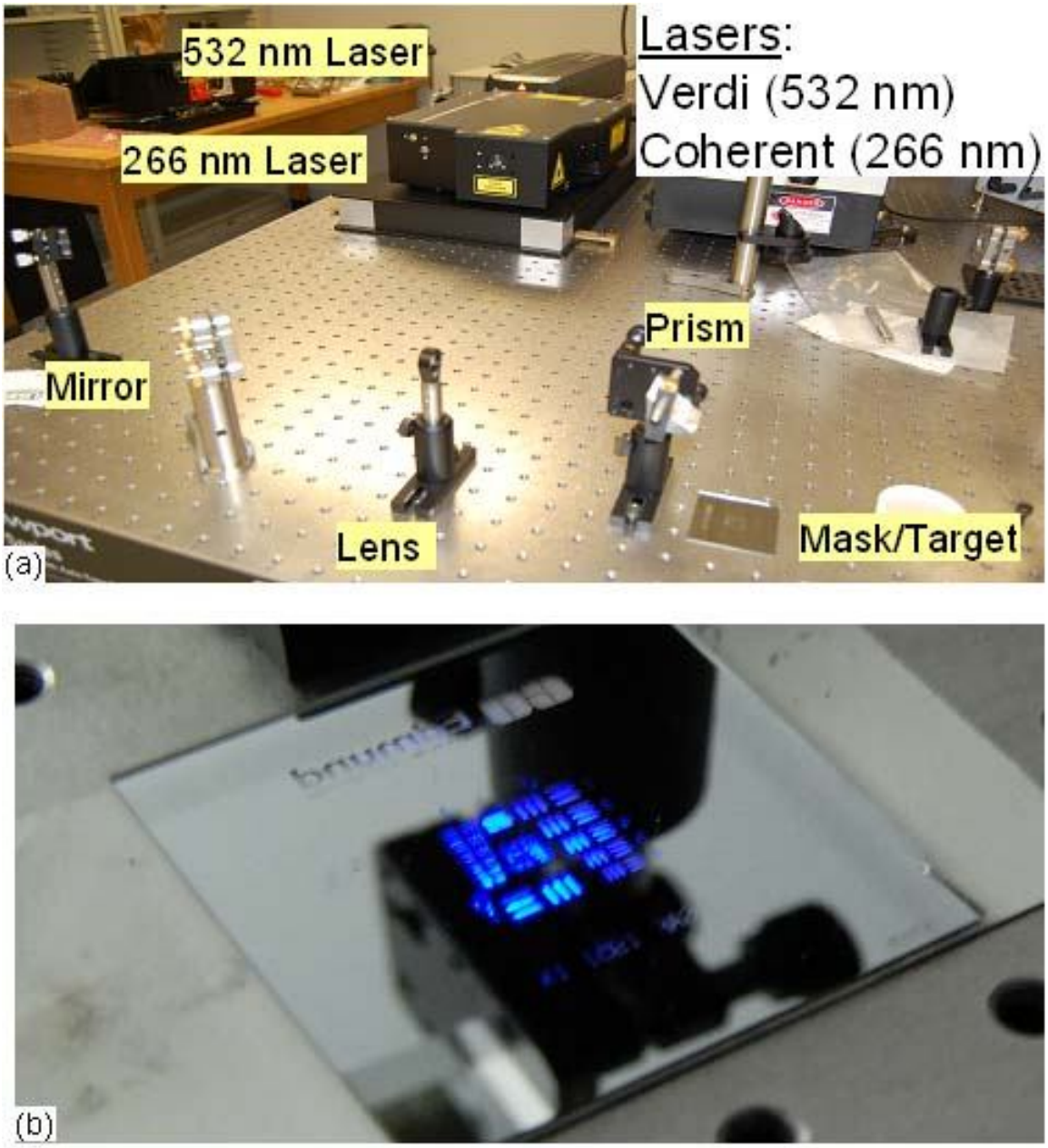

Fig. 1.4: (a) Laser set-up and (b) illuminated mask+target during exposure.

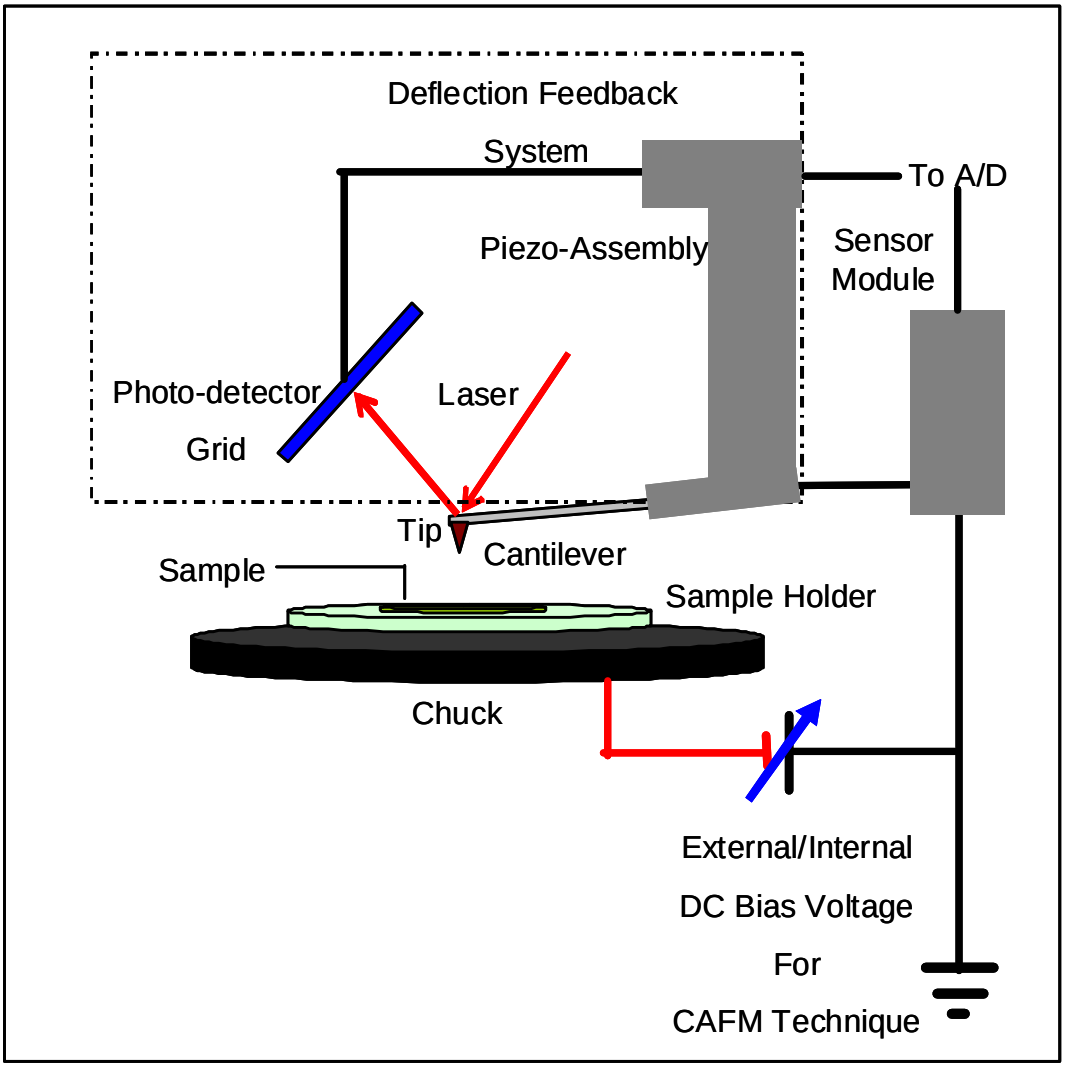

Fig. 1.5: Schematic of AFM with CAFM capability.

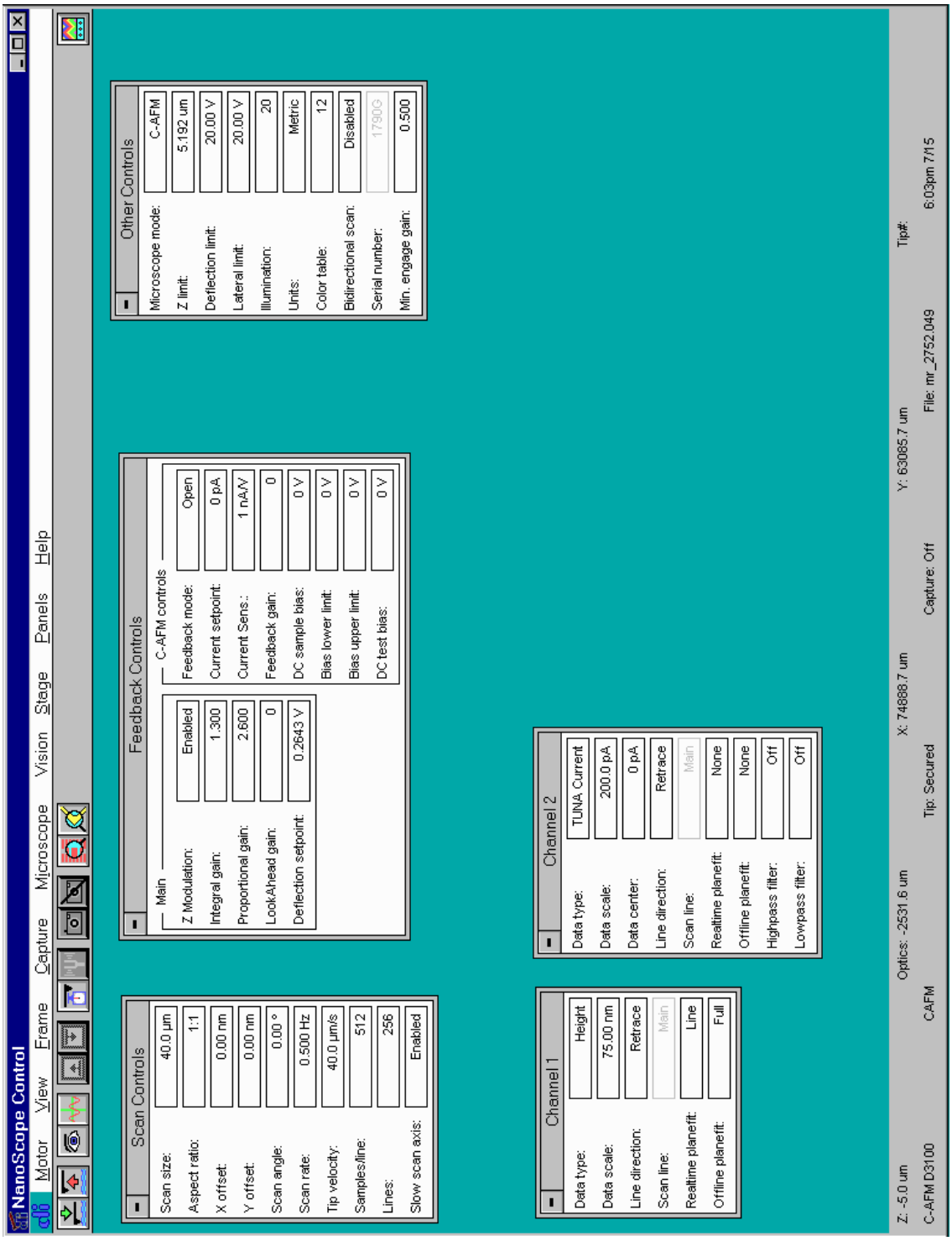

Fig. 1.6: Screen Capture of Conductive AFM for Veeco Dimension III (DIII).

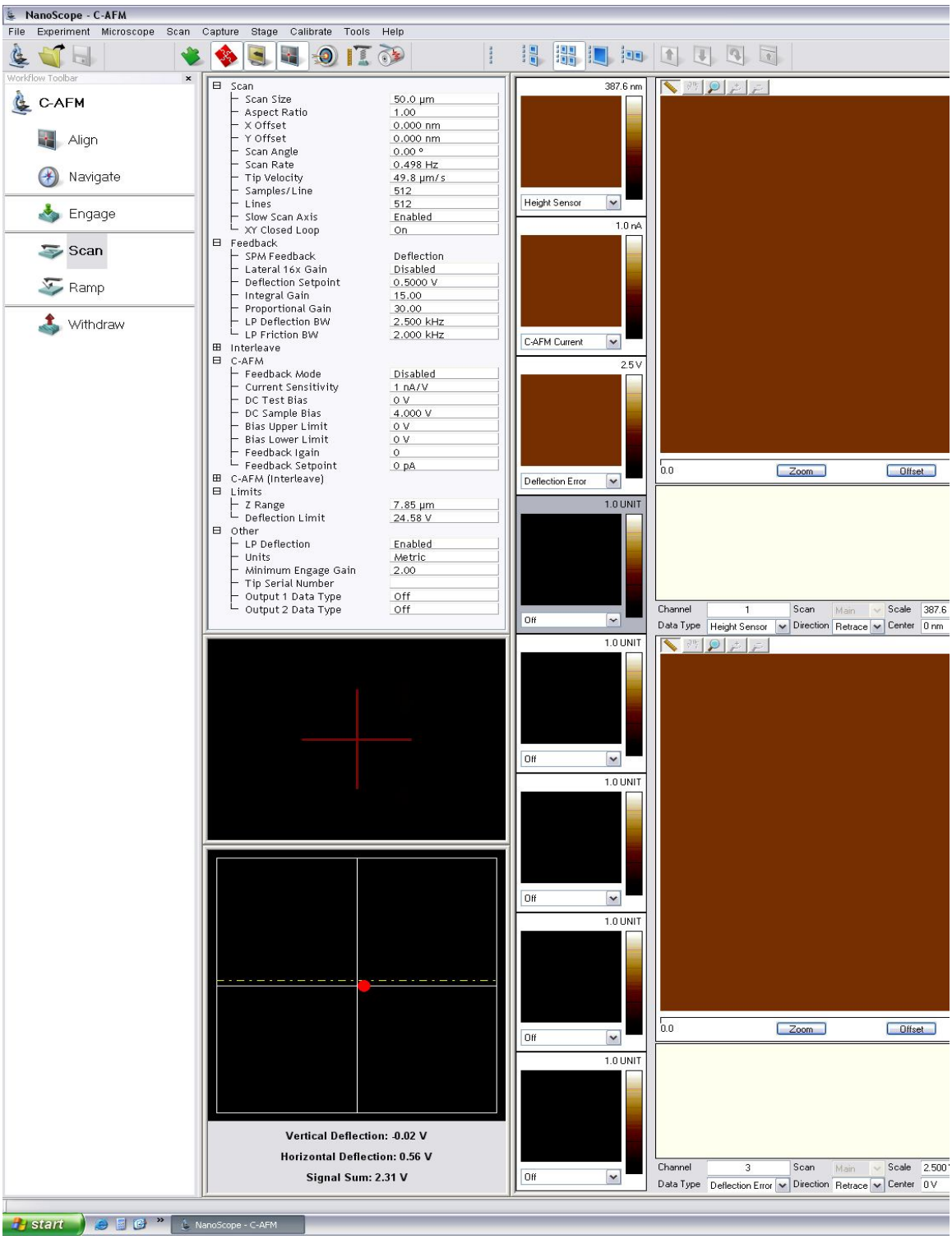

Fig. 1.7: Screen Capture of Conductive AFM for Veeco Icon.

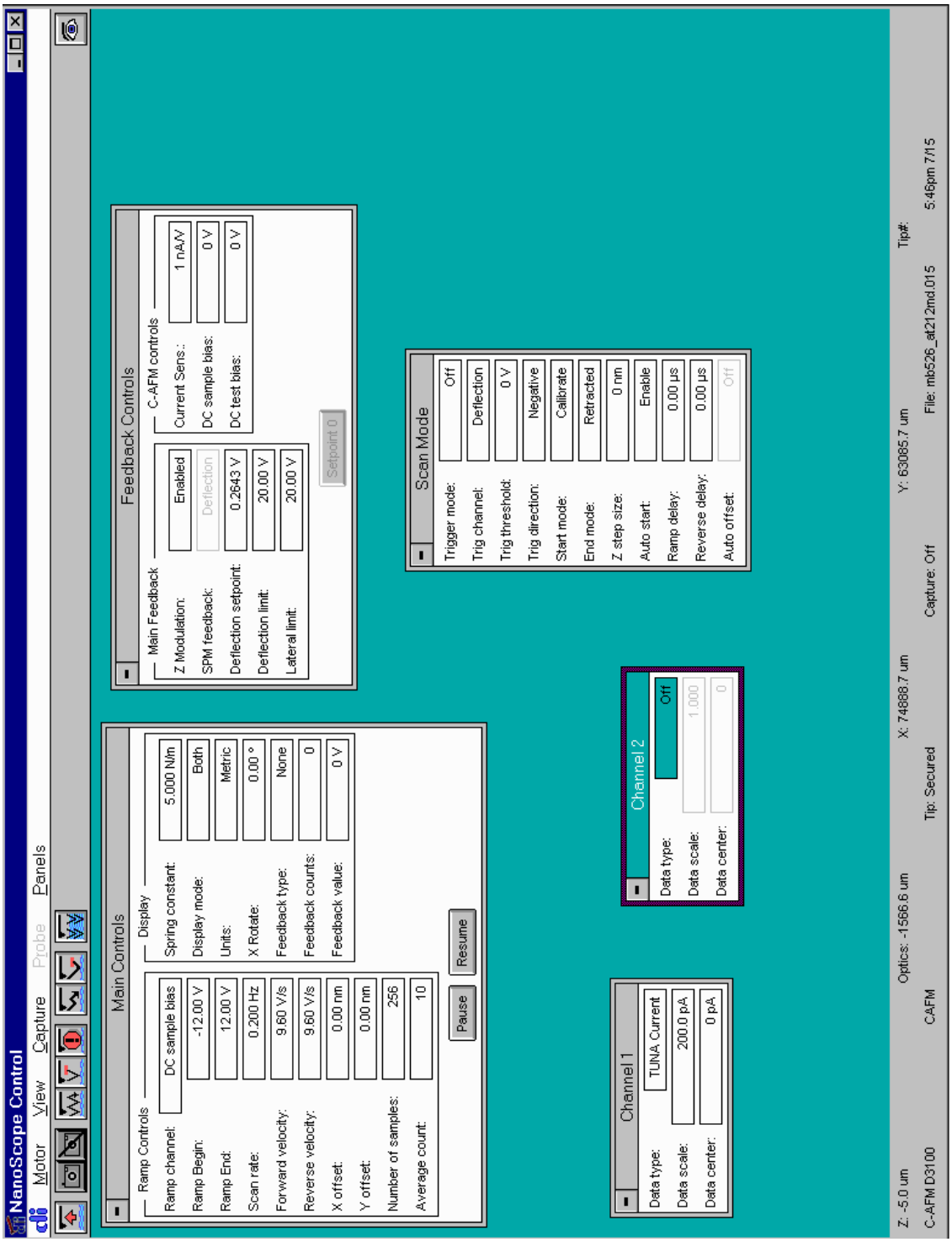

Fig. 1.8: Screen Capture of Advanced Force Mode for CAFM-IV on Veeco DIII.

Chapter 2: Formation of Ag Nanoclusters

2.1 Introduction

Photoreduction of Ag^+ to Ag has been known for some time and recently it has been used to prepare composites with multiple functionalities, as shown by the Dunn Group.[13] Ag atoms are generated by photoreduction, and typically aggregate to form nanoparticles, which are best revealed by Transmission Electron Microscopy (TEM). Ag nanoparticle formation was also detected indirectly by UV-Vis spectroscopy. In this study, three 1 M samples were made on glass slides with the following exposure times: no laser exposure, 3 min., and 45 min. Samples taken for longer exposures showed a broad absorption maximum centered around 420 nm. Silver nanoclusters are of interest because their surface plasmon resonance is in the visible region of the optical spectrum.[14] Surface plasmon resonance has frequently been applied to the characterization of thin films.[15] The broadening of the absorption at longer wavelengths indicates aggregation of the nanoparticles, which is also evident from TEM images. To determine the thickness of the films a profilometer was used.

It should be noted that x-ray diffraction (XRD) was attempted to help confirm the presence of Ag nanoclusters, but was not successful. This could be due to the films being so thin and the concentration of Ag being so low that the x-rays passed through the film. Another attempt was made by allowing the sol-gel to solidify and then be ground into a powder. The powder was then exposed to UV for an extended period of time, but there were still no XRD peaks.

2.2 Transmission Electron Microscopy and Profilometry

A TEM (Philips EM-300) was used to optically view the formation of Ag nanoclusters within the thin film. For TEM, films were scratched from glass substrates with a razor blade, and the resulting powder was deposited on carbon-coated copper grids. The two films imaged here had 3 min. and 45 min. exposures. The Ag clusters formed upon irradiation become embedded into the silica matrix.[8] As shown in Fig. 2.1, the 3-min. film appears uniform with cluster sizes of about 5 nm. The 45-min. film in Fig 2.2 shows an increased density of clusters with larger sizes in the 10-15 nm range. With increasing exposure time it appears that the Ag+ ions agglomerate into nanoclusters that grow in number and in size (to some maximum). The Ag nanoclusters do not continue to agglomerate further because the their surfaces are surrounded by some fraction of silica and of air (or solvent).[16] With a large number of open pore sites the diffusion of Ag is limited. This is why we see a peak of 15 nm clusters and nothing larger.

To measure the film thickness, a profilometer was used with a vertical resolution of tens of nanometers. A scratch was made into the film down to the Si substrate and then a diamond stylus (tip radius of ~20 nm) was moved laterally across the scratch. The profilometer scan indicated a film thickness of ~ 375 nm (see Fig. 2.3) with a uniform surface.

2.3 Ultraviolet - Visible Spectroscopy (UV-Vis)

UV-Vis spectroscopy is a technique used to find material absorbance at specific wavelengths, where noble metal nanoclusters can be characterized by a strong surface plasmon absorption band.[17] Classically, this surface plasmon band is attributed to collective oscillations of the conduction electrons in response to optical excitation.[18] In Fig. 2.4 measurements were done for samples with no laser exposure, 3 min., and 45 min. exposure on a Hewlett-Packard 8452A Diode Array Spectrophotometer. Generally, the unmodified and 3 min. films had no spectral

peaks, indicating that Ag clusters were not present. The 45 min. sample, however, had a brown tint and displayed a large absorption peak at ~ 420 nm. This peak corresponds to the formation of Ag nanoclusters and confirms our TEM results. Nanoclusters grown inside the pores affect the optical properties but not the mechanical properties.[19]

There was some difficulty with UV-Vis spectroscopy involving our glass slides. The samples were not quite large enough for the aperture of the beam. Also, the glass slides did not produce a uniform film like Si substrates. There were areas on the glass slide that were darker while others were completely transparent. Going back to the TEM images briefly, note that there are a few clusters at 3 min. exposure but that there is no UV-Vis peak. The absence of a peak could result from the sample not being sufficiently large to cover the aperture and sample non-uniformity. There should have been a gradual growth of a peak at ~ 420 nm due to the increasing formation of clusters as UV exposure time increased.

Chapter 2 Figures:

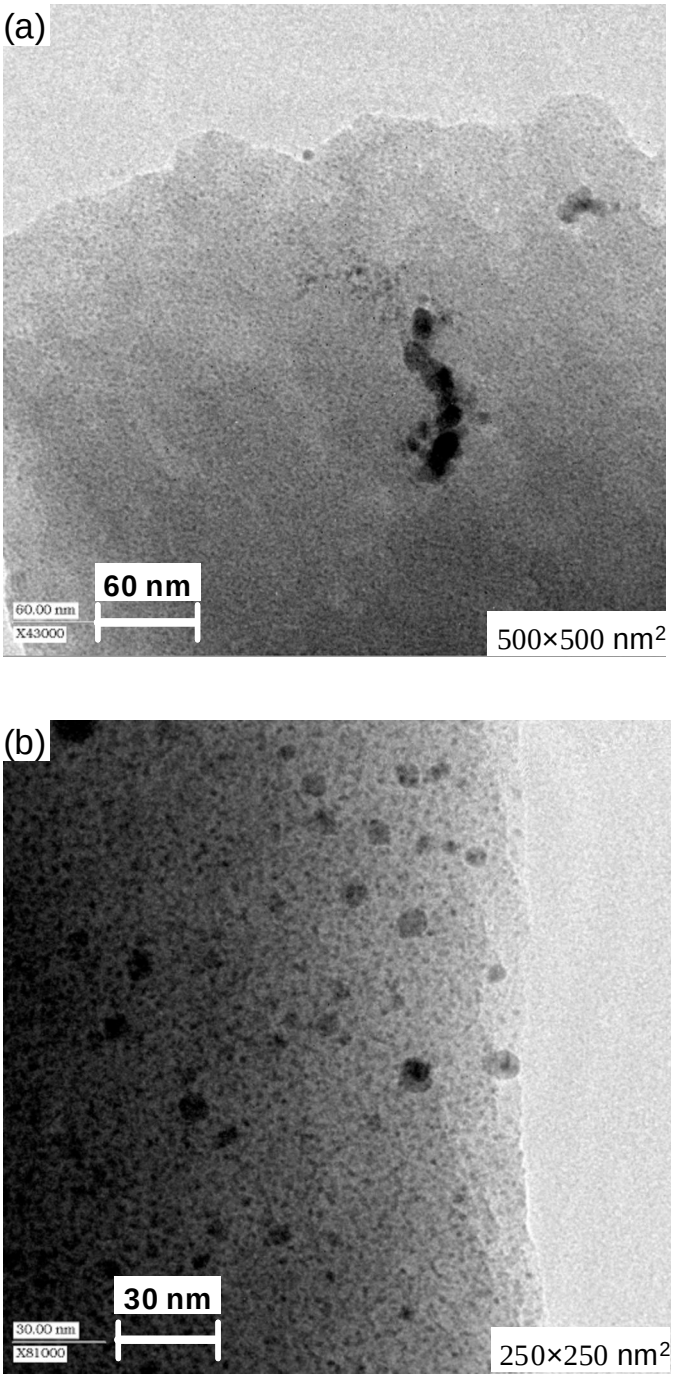

Fig. 2.1: TEM image of thin film on glass substrate (3 min. exposure at 125 mW).

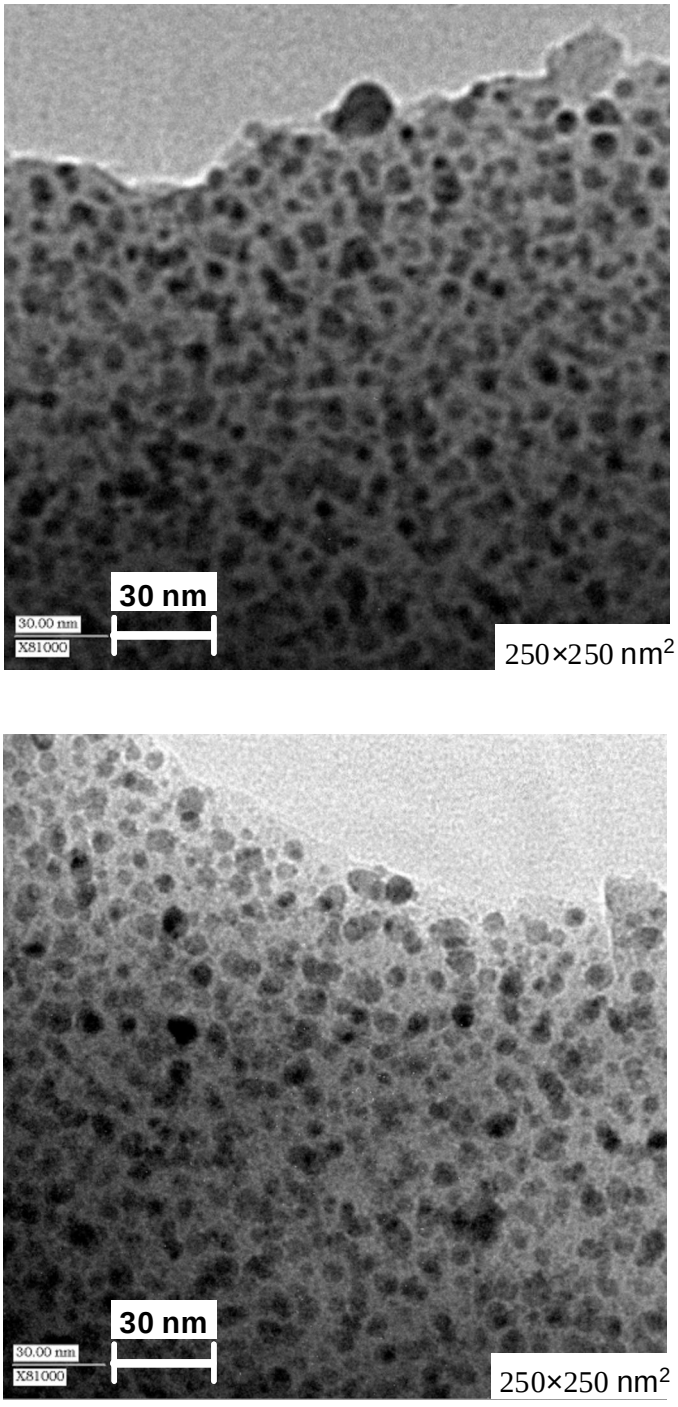

Fig. 2.2: TEM image of thin film on glass substrate (3 min. exposure at 125 mW).

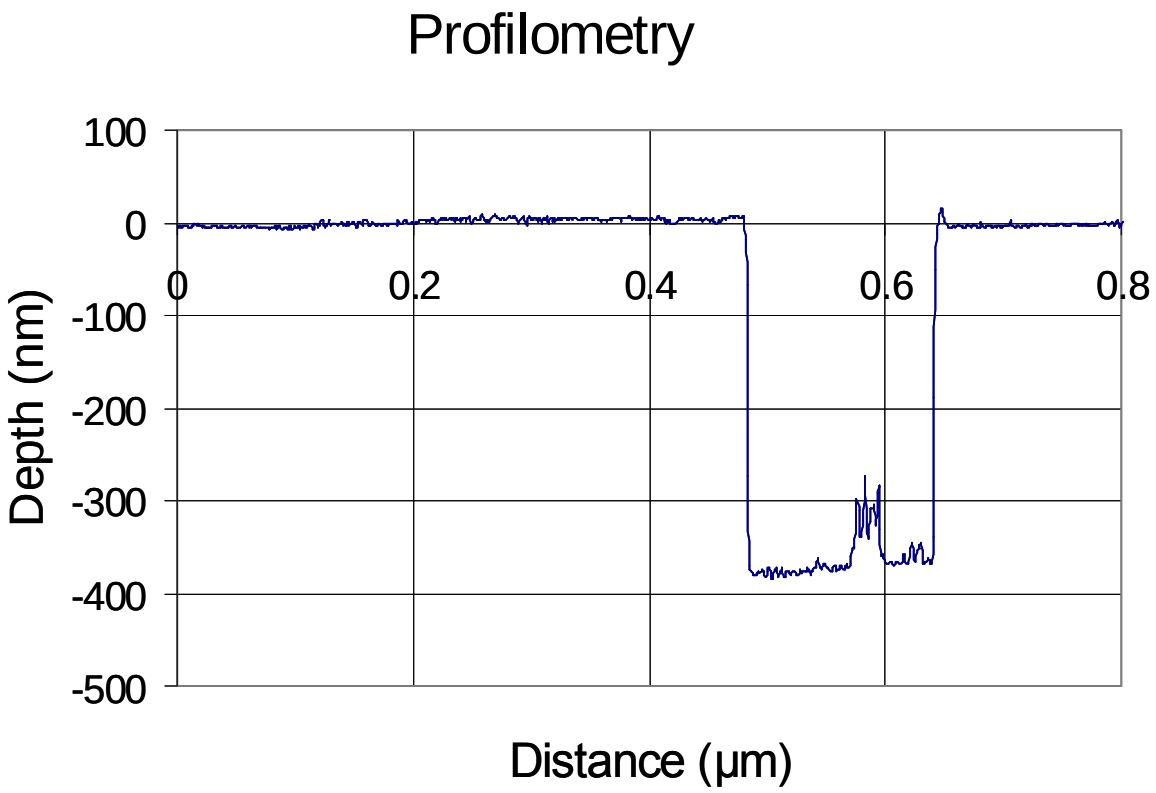

Fig. 2.3: Thin film scratched to the Si substrate to measure film thickness of ~ 375 nm.

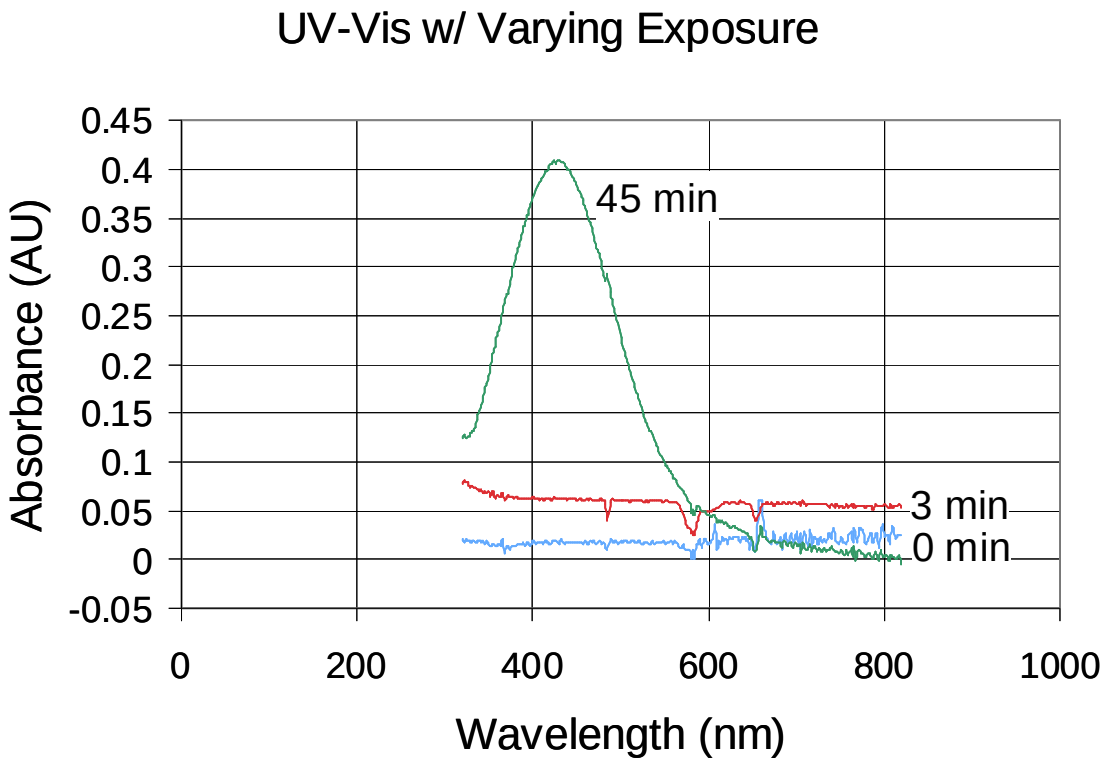

Fig. 2.4: UV-visible spectroscopy of glass thin films for no laser exposure, 3 min., and 45 min.

Chapter 3: Morphology and Conductivity of Patterned Films

3.1 Patterning Mask

The mask used for patterning during UV exposure consisted of sets of three lines of varying lengths and widths (see Fig. 3.1, USAF 1951 2", Model 57895 Edmund Optics). Surface phototransformation methods applied through a mask[20] have been used to achieve patterned deposition of a variety of biological and synthetic materials, including proteins, DNA, cells, and nanoparticles. The feature size of the mask pattern and wavelength of incident light govern the resolution of such patterns.[21] The mask is made of quartz with an aluminum top surface, where exposed regions correspond to open slits. In order to obtain high-resolution exposed patterns, it is necessary to place the aluminum surface in contact with the xerogel film. This geometry reduced laser scattering and aberrations to create a sharper exposed image on the sample.

3.2 AFM/CAFM Data

To detect the conductivity of exposed regions as a function of Ag molarity and exposure time, AFM/CAFM data were simultaneously acquired on a variety of samples. Fig. 3.2 shows a 2 M $AgNO_3$ sample exposed for 7 min. taken at a sample bias voltage of +2V. The dark regions in the AFM topography images (left) are the exposed regions of the film and are ~60 nm lower than the surrounding unexposed regions. The change in topography could be a result of the final stage of drying as the liquid-vapor menisci recede into the film interior.[22] This can create a weakening of the structure and the appearance of a depression. In the CAFM current image, the dark regions also correspond to exposed areas and indicate insulating behavior with no current conduction. The surrounding unexposed regions for this particular molarity and sample bias have

a current of 15 pA. Note that defects such as the protrusion in Fig. 3.2c (adjacent to "6") usually appear with the same conducting behavior as surrounding regions. This defect behavior demonstrates that topography effects are minimal in the CAFM current image, i.e., both high and low topography features result in the same measured current.

Fig. 3.3 shows another set of AFM and CAFM images taken for a 1 M AgNO3 sample exposed for 8 min. at a sample bias voltage of +4 V. It is interesting to note that interference fringes are visible both between and within exposed regions, producing linear features with a spacing of only a micron or less. This interference phenomenon demonstrates the resolution of the CAFM technique and confirms that vibrations were minimal during exposure. Similar results are shown for a 9-minute exposure sample in Fig. 3.4.

It is interesting to note that these films can be lithographically 'exposed' using the CAFM tip, most notably for high molarity samples. The tip-sample current during CAFM measurements can cause the film to become optically dark and eventually become insulating in scanned regions. Similar to UV exposure, the tip-sample current appears to cause Ag nanocluster aggregation and decrease the local conductivity.

3.3 Current-Voltage Data

In this study, the sample conductivity was measured both as a function of $AgNO_3$ molarity and UV exposure time. The time intervals for UV exposure were 0, 1, 2, 3, 4, and 8 min. and molarities of 0.1 M and 1 M were measured. Fig. 3.5 shows CAFM current-voltage spectra for (a) 0.1 M and (b) 1 M with increasing exposure times. The 0.1 M sample has a minimum voltage for current conduction of approximately 8 V for all exposure times, whereas the 1 M sample has a minimum voltage for conduction of 1 V to 6 V for 0 min. to 8 min exposure time, respectively. The maximum current for the unexposed 0.1 M sample is ~25 pA at 12 V, and for the unexposed

1 M sample is the current limit of the amplifier (100 pA) at 8 V. In all cases, as the UV exposure time increases, the sample conductance decreases until it becomes very low (<10 pA) for times over 3 min. (see Fig. 3.6).

These I-V data confirm the formation of Ag nanoclusters. Initially, Ag ions are evenly distributed throughout the film and it is conducting. As the film is exposed to UV, Ag clusters form which have relatively large spacings that disrupt current conduction, i.e., the film is no longer a percolated network. As expected, the higher molarity films are initially more conducting but they also become insulating after only ~3 min. UV exposure.

3.4 Non-standard Behaviors

It should be noted that when sample preparation is altered from the procedures outlined in Chapter 1, the results can be different from what is expected. It is important that the sample be allowed to "age" in a dark area for one day in order to allow any excess solvent and water to evaporate. If the sample is immediately exposed to UV after preparation, it is not properly stabilized and has unpredictable topography and conduction properties. For example, as shown in Fig. 3.7, exposed regions can have a higher topography and higher conduction, instead of the expected lower topography and lower conduction. It cannot be overemphasized the importance of properly "aging" samples before UV exposure.

3.4 Concluding Remarks

We have demonstrated the successful production of patterned xerogel thin films using silver and a dip-coating process. The film thickness is ~ 375 nm with a relatively uniform surface. Ag^{+} ions can be photoreduced to Ag metal using UV exposure and form Ag nanoclusters. These nanoclusters were confirmed with transmission electron microscopy and UV-Vis spectroscopy.

For patterned samples, the exposed areas have lower topography and insulating properties and demonstrate a resolution of a few microns. This process allows for the ability to “tune” the conductance of the sample with exposure time.

Chapter 3 Figures:

(a)

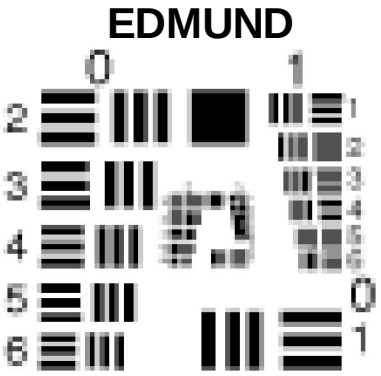

(b)

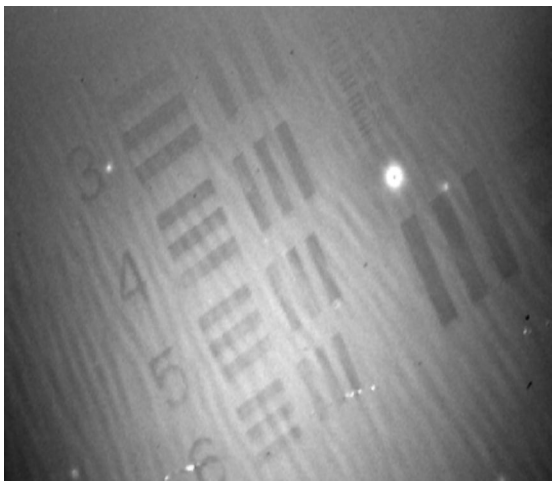

Fig. 3.1: (a) Edmund Optics USAF 1951 2” Target. (b) Digital camera image of the mask.

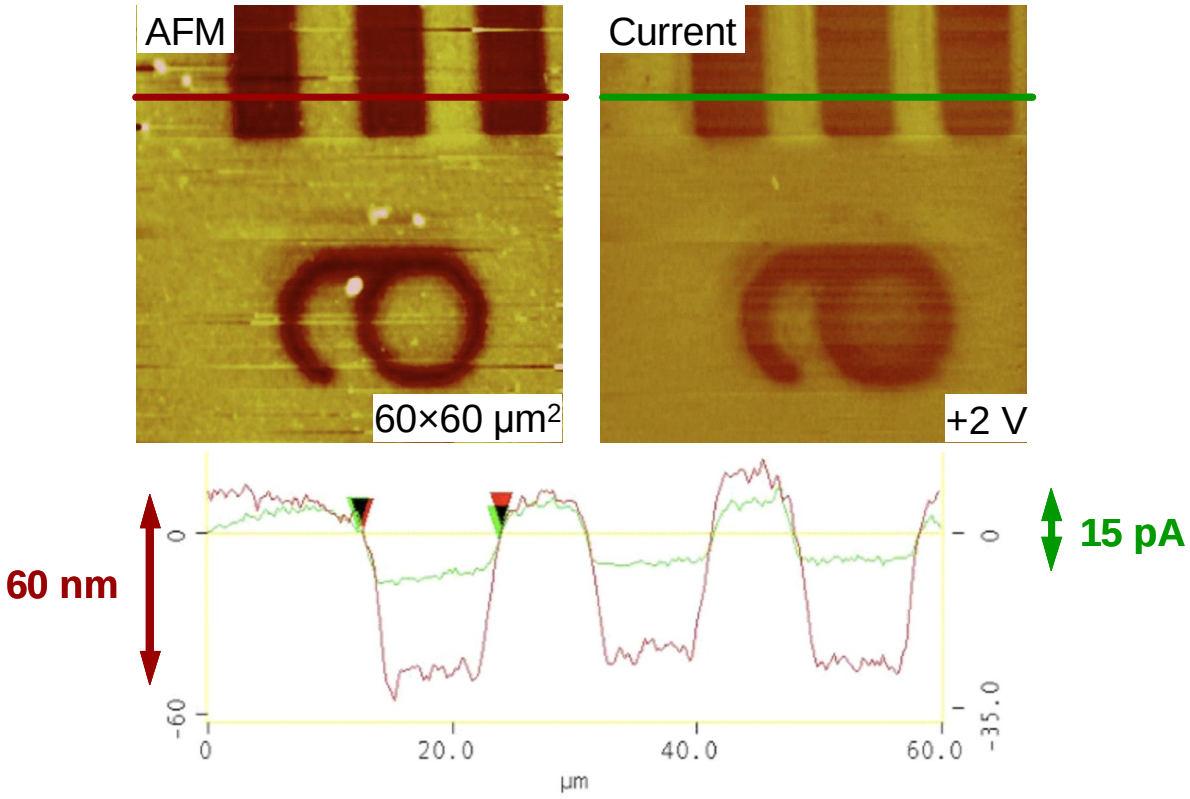

Fig. 3.2: (a,c) AFM topography and (b,d) CAFM current images of indicated samples. (c) Cross-section corresponding to line in (c,d).

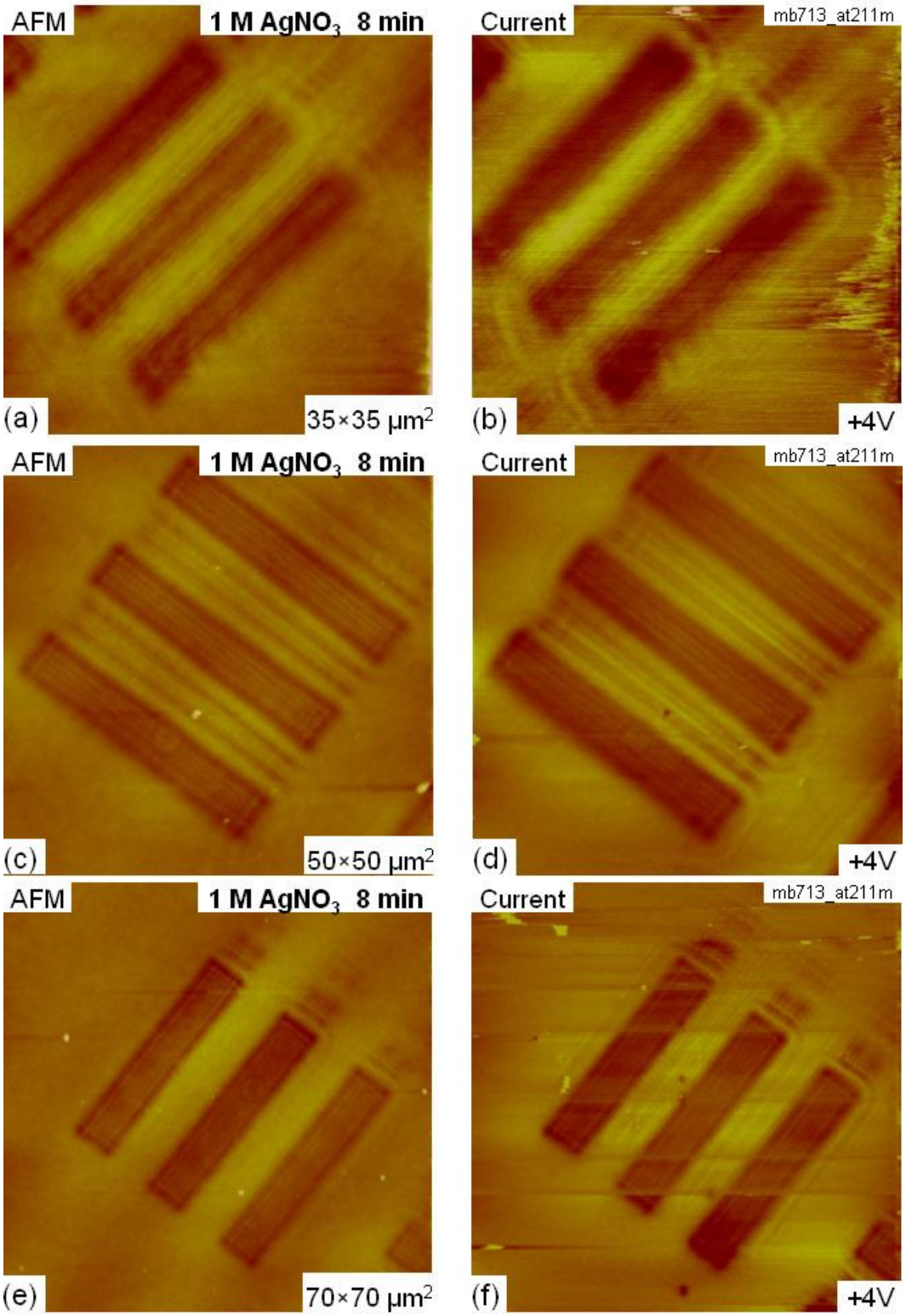

Fig. 3.3: (a,c,e) AFM topography and (b,d,f) CAFM current images of 1 M samples with 8 min. exposure time.

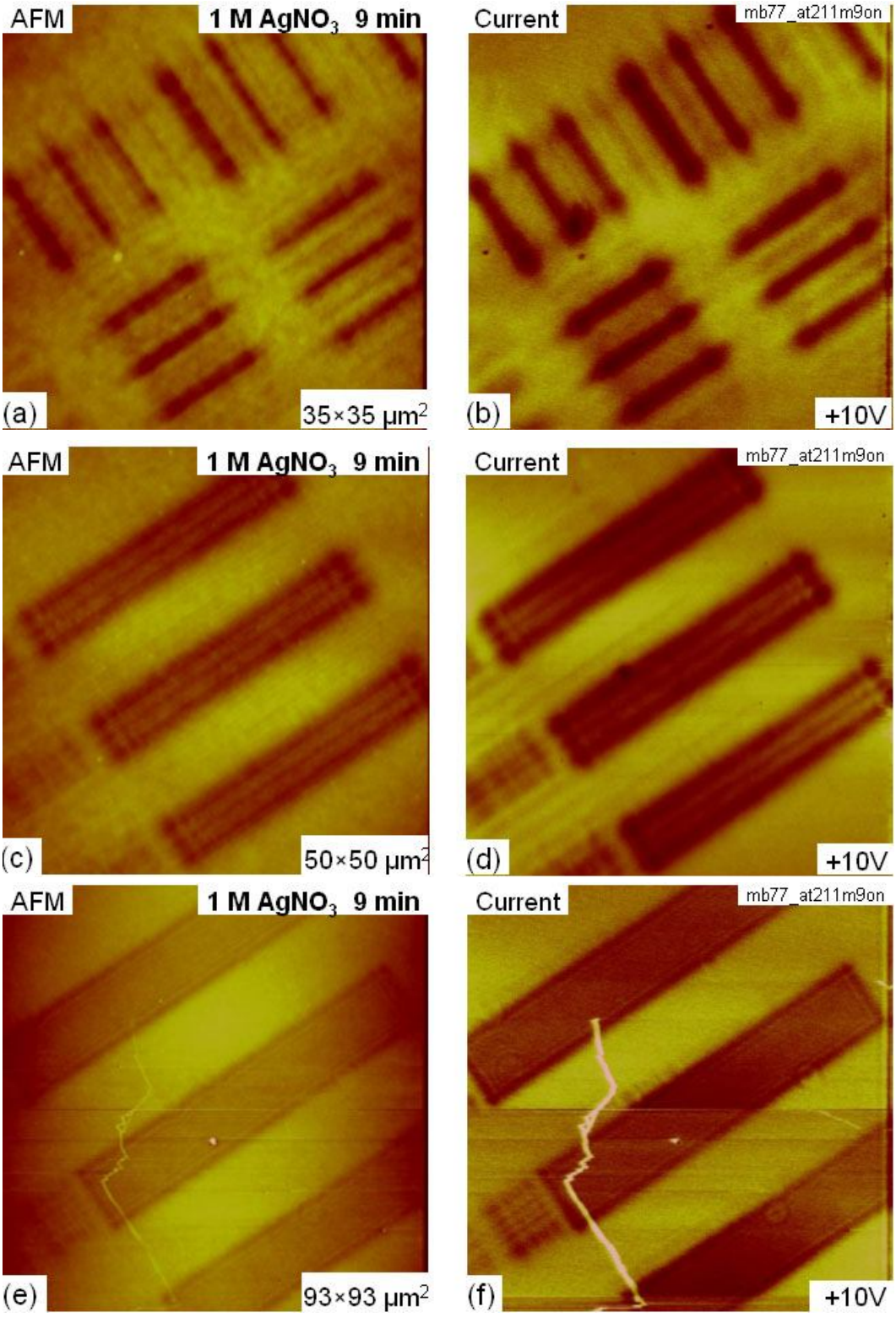

Fig. 3.4: (a,c,e) AFM topography and (b,d,f) CAFM current images of 1 M samples with 9 min. exposure time.

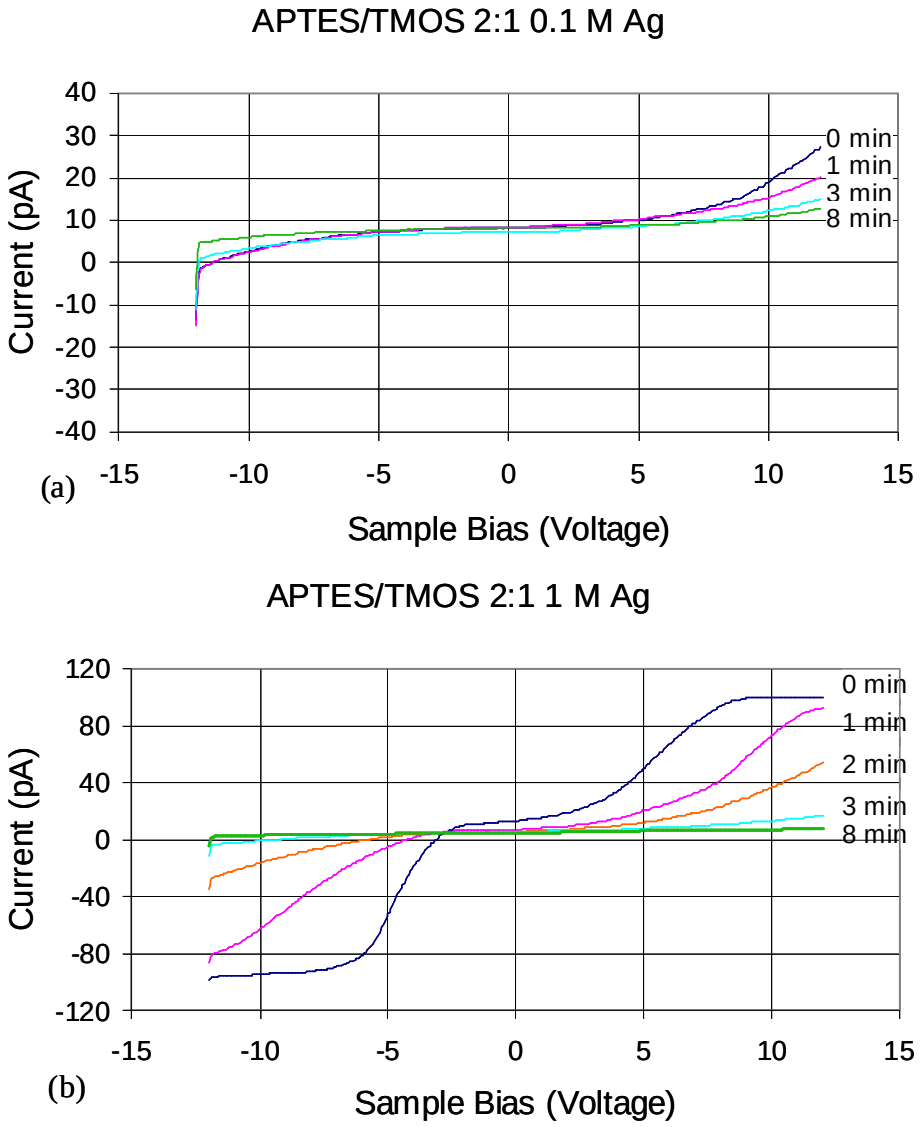

Fig. 3.5: CAFM I-V data for different exposure times for (a) 0.1 M and (b) 1 M samples.

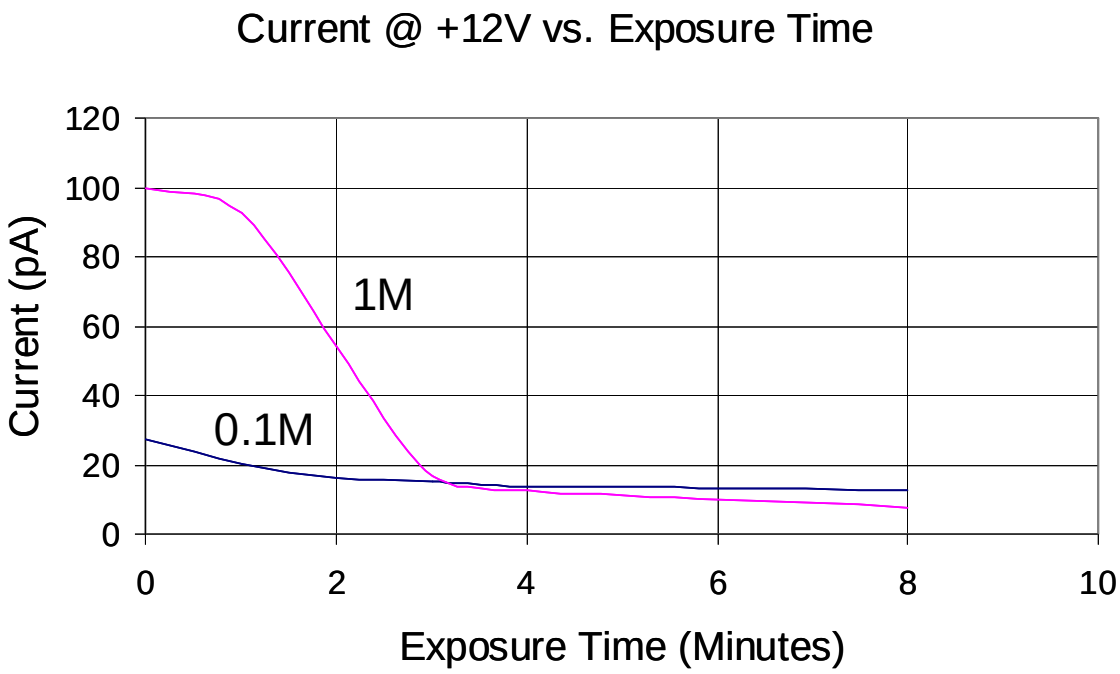

Fig. 3.6: Graph of current vs. exposure time (125 mW) for 1 M and 0.1 M samples.

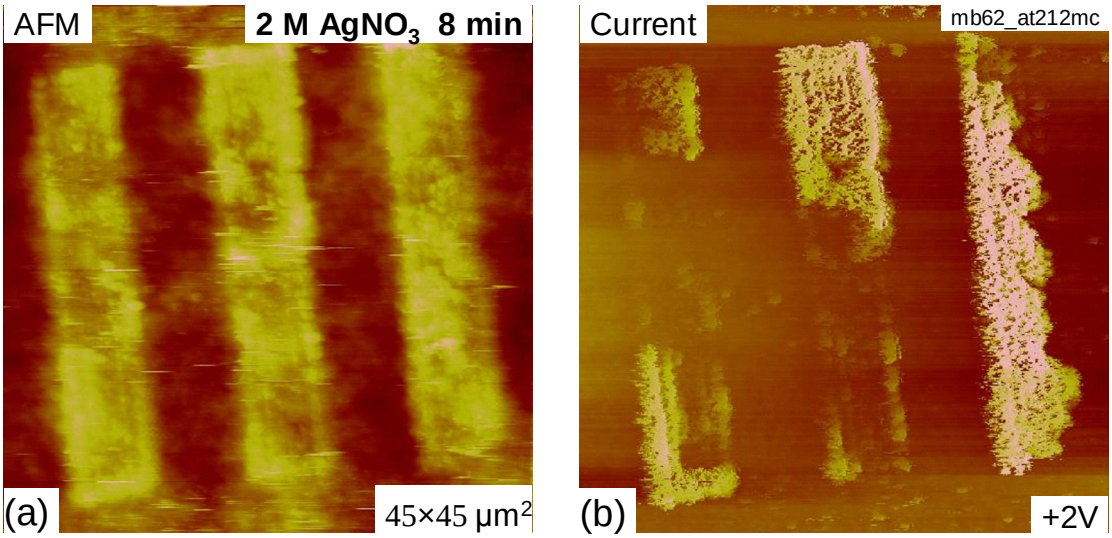

Fig. 3.7: (a) AFM topography and (b) CAFM current images of 2 M samples with 8 min. exposure time that demonstrates abnormal behavior for improperly prepared samples.

References

[1] Pierre, A. C.; Pajonk, G. M. *Chem. Rev.* 102, 4243 (2002).

[2] Wu, P.-W.; Cheng, W.; Martini, I. B.; Dunn, B.; Schwartz, B. J.; Yablonovitch, E. *Adv. Mater.* 12, 1438 (2000).

[3] Bertino, M. F.; Gadipalli, R. R.; Story, J. G.; Williams, C. G.; Zhang, Z.; Sotiriou-Leventis, C.; Tokuhiro, A. T.; Guha, S.; Leventis, N. *Appl. Phys. Lett.* 85, 6007 (2004).

[4] Bertino, M. F.; Gadipalli, R. R.; Martin, L. A.; Rich, L.E.; Yamilov, A.; Heckman, B. R.; Leventis, N.; Guha, S.; Katsoudas, J.; Divan, R.; Mancini, D. C. *Nanotechnology* 18, 315603 (2007).

[5] Yang, P.; Wirnsberger, G.; Huang, H. C.; Cordero, S. R.; McGehee, M.D.; Scott, B.; Deng, T.; Whitesides, G. M.; Chmelka, B.F.; Buratto, S. K.; Stucky, G. D. *Science* 287, 465 (2000).

[6] Uhlmann, D. R.; Suratwala, T.; Davidson, K.; Boulton, J. M.; Teowee, G. *J. Non-Cryst. Solids 218*, 113 (1997).

[7] Bhave, R.R. In *Inorganic Membranes Synthesis and Applications*; Van Nostrand Reinhold: New York, p. 1 (1991).

[8] S.P. Ramnani et al. / *Radiation Physics and Chemistry* 76, 1290-1294 (2007).

[9] Henglein, A., Colloidal silver nanoparticles: photochemical preparation and interaction with O_2, CCl_4 and some metal ions. Chem. Mater. 10, 444-450 (1998).

[10] L.E. Scriven, in: Better Ceramics Through Chemistry III, eds. C.J. Brinker, D.E. Clark and D.R. Ulrich (Mater. Res. Soc., Pittsburgh, PA, 1988) p. 717.

[11] C.J. Brinker, A.J. Hurd and K.J. Ward, in: Ultrastructure Processing of Advanced Ceramics, eds. J.D. Mackenzie and D.R. Ulrich (Wiley, New York, 1988) p. 223.

[12] Y. Martin, C.C. Williams, H.K. Wickramasinghe, *J. Appl. Phys.* 61, 4723 (1987).

[13] Wu, P.-W.; Cheng, W.; Martini, I. B.; Dunn, B.; Schwartz, B. J.; Yablonovitch, E. *Adv. Mater.* 12, 1438 (2000).

[14] T.H. Lee, J.I. Gonzales, R. Dickson, Proc. Natl. Acad. Sci. 99, 10272 (2002).

[15] H. Knobloch, G.V. Szada-Borryszkowski, S. Woigk, A. Helms, L. Brehmer, Appl. Phys. Lett. 69, 2336 (1996).

[16] D.D. Smith et al. *J. Non-Crystalline Solids* 225, 330-334 (1998).

[17] C. Sonnichsen, T. Franzl, T. Wilk, G. von Plessen, J. Feldmann, New J. Phys. 4, 93.1 (2002).

[18] C.F. Bohren, D.R. Huffman, Absorption and Scattering of Light by Small Particles, Wiley, New York, 1983.

[19] Heckman, B.; Martin, L.; Bertino, M. F.; Leventis, N.; Tokuhiro, A. T. *Sep. Sci. Technol.* 43, 1474 (2008).

[20] M.J. Madou, *Fundamentals of Microfabrication*, CRC Press, New York, 2002.

[21] E.J. Park, G.T. Carroll, N.J. Turro, J.T. Koberstein. *Soft Matter* **5**, 36-50 (2009).

[22] C.J. Brinker, G.C. Frye, A.J. Hurd, K.J. Ward and C.S. Ashley, in: Proc. 4th Int. Conf. on Ultrastructure Processing of Glasses, Ceramics and Composites, eds. D.R. Uhlmann and D.R. Ulrich (Wiley, New York, 1990) in press.